Analysis of the Effect of Osteon Diameter on the Potential Relationship of Osteocyte Lacuna Density and Osteon Wall Thickness

JOHN G. SKEDROS,[1]* **GUNNAR C. CLARK,**[1] **SCOTT M. SORENSON,**[1]
KEVIN W. TAYLOR,[1] AND **SHIJING QIU**[2]

[1]Department of Veterans Affairs Medical Center, Bone and Joint Research Laboratory,
and University of Utah, Salt Lake City, Utah
[2]Bone and Mineral Research Laboratory, Henry Ford Hospital, Detroit, Michigan

ABSTRACT

An important hypothesis is that the degree of infilling of secondary osteons (Haversian systems) is controlled by the inhibitory effect of osteocytes on osteoblasts, which might be mediated by sclerostin (a glycoprotein produced by osteocytes). Consequently, this inhibition could be proportional to cell number: relatively greater repression is exerted by progressively greater osteocyte density (increased osteocytes correlate with thinner osteon walls). This hypothesis has been examined, but only weakly supported, in sheep ulnae. We looked for this inverse relationship between osteon wall thickness (On.W.Th) and osteocyte lacuna density (Ot.Lc.N/B.Ar) in small and large osteons in human ribs, calcanei of sheep, deer, elk, and horses, and radii and third metacarpals of horses. Analyses involved: (1) all osteons, (2) smaller osteons, either ≤ 150 μm diameter or less than or equal to the mean diameter, and (3) larger osteons (>mean diameter). Significant, but weak, correlations between Ot.Lc.N/B.Ar and On.W.Th/On.Dm (On.Dm = osteon diameter) were found when considering all osteons in limb bones (r values -0.16 to -0.40, $P < 0.01$; resembling previous results in sheep ulnae: r = -0.39, $P < 0.0001$). In larger osteons, these relationships were either not significant (five/seven bone types) or very weak (two/seven bone types). In ribs, a negative relationship was only found in smaller osteons (r = -0.228, $P < 0.01$); this inverse relationship in smaller osteons did not occur in elk calcanei. These results do not provide clear or consistent support for the hypothesized inverse relationship. However, correlation analyses may fail to detect osteocyte-based repression of infilling if the signal is spatially non-uniform (e.g., increased near the central canal). Anat Rec, 294:1472–1485, 2011. © 2011 Wiley-Liss, Inc.

Key words: osteons; osteocytes; osteon wall thickness; bone remodeling; sclerostin

The process of remodeling in cortical and cancellous bone is important for ensuring the maintenance of mechanical competence and calcium balance (Frost, 1990; Parfitt, 1994). In this context, "remodeling" refers to the formation of complete secondary osteons (Haversian systems) in cortical bone and hemiosteons in cancellous bone (Parfitt, 1994). The remodeling process is characterized by the coupled actions of osteoclasts (bone resorption) and osteoblasts (bone formation). These cells comprise the basic multicellular units that mediate the activation–resorption–formation (A–R–F) sequence that results in secondary osteons, or basic structural units (Frost, 2001; Cooper et al., 2006). Osteocytes, the most prevalent cell type in bone, are thought to be important in mechano-sensation/mechano-transduction (Marotti et al., 1992; Burger and Klein-Nulend, 1999; Weinbaum et al., 2001; Riddle and Donahue, 2009; Herman et al., 2010).

Although most osteoblasts involved in osteon formation are not accounted for at the termination of infilling (they presumably undergo apoptosis; Parfitt, 1994), the remainder differentiate into osteocytes as they become embedded in the newly formed matrix; their cell bodies being contained within osteocytic lacunae (ellipsoid cavities). Marotti (1996) hypothesized that during the formation of secondary osteons, the newly formed osteocytes send inhibitory signals to surrounding osteoblasts. This signal causes the osteoblasts to cease bone formation. Recent studies of the mechanical stimulation of bone have suggested that this inhibitory effect is regulated by the expression of the SOST gene, which is responsible for the formation of sclerostin, an osteocyte-specific glycoprotein involved in the inhibition of osteoblasts (Van Bezooijen et al., 2004; Robling et al., 2008; Turner et al., 2009). Experimental evidence suggests that sclerostin is produced by osteocytes that are within well mineralized matrix (Irie et al., 2008).

Before recognition of the importance of sclerostin in bone remodeling, Martin expanded on this osteocyte inhibitory concept with his "unifying theory of bone remodeling," wherein osteoblast activity is controlled by osteocytes via signaling through their interconnected network. More specifically, osteoblasts remaining at the termination of osteon infilling (i.e., termination of osteon wall formation) differentiate into a distinct cell type— bone lining cells (BLCs; Martin, 2000a,b). In turn, the BLCs maintain communication with the embedded osteocytes via gap junctions (Fig. 1). At the termination of osteon infilling, instead of regulating osteocyte formation, the interconnected osteocytes, in theory, send inhibitory signals to the BLCs to suppress the activation of that would lead to a new remodeling cycle (Stages 8 and 1 in Table 1). Martin (2000b) further hypothesized that the strength of the inhibitory signal is proportional to the number of osteocytes in communication with the BLCs.

Experimental data reported by Metz et al. (2003) in ulnae of adult sheep provide indirect support for the idea that the osteocyte network regulates the rate and duration of osteon infilling (Fig. 2). However, although their data revealed an inverse relationship between osteon wall thickness (On.W.Th) and osteocyte lacuna density (Ot.Lc.N/B.Ar; B.Ar = bone area within a secondary osteon), it was weak (r = −0.39, P < 0.0001). Nevertheless, these authors concluded that it was biolog-
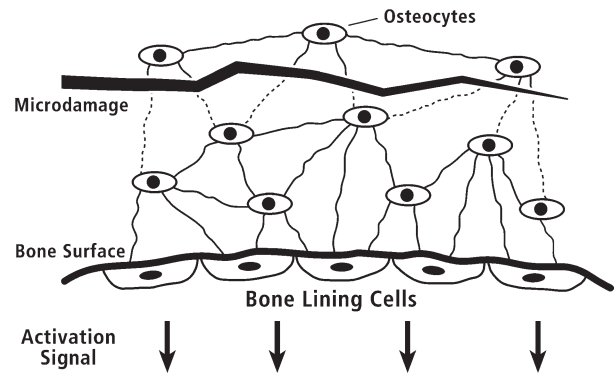

Fig. 1. Schematic diagram of the proposed mechanism for the control of activation of bone remodeling. Within the bone tissue at "top," the elliptical objects represent osteocytes. The heavy line at "bottom" indicates a quiescent (not remodeling) bone surface; five BLCs are shown on this surface. The multiple thin lines connecting the osteocytes to one another and to the BLCs schematically represent cell processes within canaliculi. The jagged horizontal line indicates microdamage (microcrack) to the calcified matrix, which interferes with the generation or transmission of the osteocytic signal. Reduced signal generation/transmission is indicated as dotted lines for the canaliculi physically disrupted by the microcrack. In theory, when these inhibitory signals fall below a threshold value, the BLCs initiate activation of remodeling. (From Martin, Bone, 2000b, 26, 1–6, Fig. 2, © Elsevier, reproduced by permission.)

ically important, supporting the hypothesis that osteocytes influence the degree of osteon infilling. Although Qiu et al. (2003) also argued in favor of this relationship in their analysis of osteons from ribs of young human males, they did not specifically consider On.W.Th, but only evaluated relationships of Ot.Lc.N/B.Ar with Haversian canal area (HC.Ar) and HC.Ar/On.Ar (On.Ar = osteon area). Both of these comparisons in human rib osteons, however, showed no or little correlation (r = 0.011 and 0.104, respectively), and only the latter is positive and statistically different from no correlation. Regardless of the specific mechanism(s) involved, Martin and coworkers' important hypothesis has not been examined in other bones and/or for potential influences of osteon size. The only studies that we could locate have examined osteons in cortices of elderly human proximal femora (no consideration for osteon size; Power et al., 2001, 2002), which could be confounded by the effects of bone disease (e.g., osteoporosis) and/or aging (Britz et al., 2009).

Influences of osteon size on the putative inverse relationship of Ot.Lc.N/B.Ar with On.W.Th could occur in proportion to the efficiency with which the proposed inhibitory signal can be transmitted from one osteocyte to another (e.g., through a neural-like network) or delivered (e.g., convective transport of sclerostin in lacunar–canalicular spaces) across the osteon wall. In a mathematical analysis dealing with the duration and extent of osteon infilling, Martin (2000a) argued that if the osteocyte-network signal decayed slowly as the osteon progressively infilled, then the strength of the inhibitory signal at the canal surface would depend on osteon size. But if the signal decayed relatively rapidly, then the signal would not increase very much once an osteon's wall exceeds ~100–120 µm (Fig. 3), constraining potential

TABLE 1. Stages of the remodeling process with the descriptions given for the most salient characteristic(s) of each stage

Stages of remodeling (the formation of secondary osteons)			
Activation		Resorption	Formation
1 Activation	2 Migration & proliferation	3 Bone resorption	4[a] Bone formation
The beginning of the process of remodeling.	Osteoclasts are recruited, migrate, and proliferate.	Formation of a resorption cavity by osteoclasts.	Osteoblasts form bone on the resorbed surface and lay down sequential lamellae. The cement line is formed first.
Formation		Quiescent stage[b]	
5[a] Differentiation Osteoblasts differentiate into osteocytes, which become embedded in the bone matrix.	6[a] Termination Formation of the central canal due to termination of infilling. (Strongly influenced by osteoblast apoptosis.)	7 Bone lining cells Blcs cover the the bone surface of the central canal.	8 Possible repression Osteocytes, via control of BLC, repress activation of a new remodeling cycle (Fig. 1).

Stages 4–6 (the formation stage) are the focus of this study because they deal with the hypothesis that osteocytes density is inversely related to the degree of osteon infilling. Another hypothesis is that osteocytes send a repressive signal to the BLCs that inhibits bone resorption (Stages 8 and 1; Fig. 1). This hypothesis was not evaluated in this study. The delineation of eight stages, as done here, serves to clarify the focus of the data analysis in this study. They are not intended to supplant the widely accepted quiescence period, then A-R-F sequence-each stage with its own well-understood and integrated cellular cascades.
BLC: bone lining cells; central canal: Haversian canal; secondary osteon: Haversian system.
[a]Stages of remodeling addressed in the current study.
[b]The quiescent stage is defined by the remaining osteoblasts becoming lining cells, and then remaining as such for some time. This stage is a complex integrative physiological state that involves osteocyte production of signals, BLC integration of those signals, and then BLC communication to endothelial cells and osteoblast and osteoclast precursors.

increases in osteon size. Similar arguments could be made on the basis of the "transport" of sclerostin via convective fluid flow through the interstitial microporosities of the osteon wall.

Regardless of the nature of the putative inhibitory "signal" and how it is "transmitted" or "delivered," we hypothesize that if it is produced by osteocytes and is negatively correlated with the degree of osteon infilling, then in fully formed osteons: (1) it should be detected as an inverse relationship between On.W.Th and Ot.Lc.N/B.Ar and (2) this inverse relationship should be influenced by osteon size.

MATERIALS AND METHODS

As detailed below, microscopic images were obtained from the ribs of young adult modern human males (20–25 years old) and various nonhuman limb bones from adult animals: (1) radii and third metacarpals (MC3s) from horses and (2) calcanei from horses, sheep, deer, and elk. These nonhuman bones had been used in our previous studies (Skedros et al., 1994a,b, 1996, 1997, 2007b; Mason et al., 1995; Skedros, 2005). The human ribs had also been used in a previous study (Qiu et al., 2003). The rationale for selecting the various nonhuman bone types is that they reflect three different loading regimens that correlate with the magnitude of neutral axis rotation during typical functional loading (Fig. 4). In turn, these regimens represent differences in load complexity from the simple cantilevered bending of the

calcanei to the increased bending/torsion of the equine MC3s. The rationale for examining the ribs is based on the fact that a great deal of what is known about basic osteon dynamics has been determined in the studies of ribs (Pirok et al., 1966; Parfitt, 1983; Qiu et al., 2003). Finally, the osteons in these bones also span a broad size range, which, as argued in our previous studies and those of others (Pfeiffer et al., 2006), reflects adaptations aimed at enhancing tissue mechanical properties for regional differences in mechanical requirements (limb bones) and/or metabolic demands (ribs).

The regions examined in the nonhuman bones are shown in Figs. 5 and 6. It must be noted that below we primarily use "anterior" and "posterior," respectively, as surrogates for the actual, but various, terms used for the opposing sagittal-plane cortices in the calcanei (dorsal and plantar), radii (cranial and caudal), and equine MC3 (dorsal and palmar).

Equine Radii and MC3s

Ten radii and nine third metacarpals (MC3s) were obtained from skeletally mature standard-bred and quarter horses with no history of racing or race training and no evidence of skeletal pathology at the time of death (Figs. 4 and 6). Only one bone was obtained from each animal. The bones had been used in previous studies reporting correlations of various material characteristics with habitual strain environments from the mid-third of the bone (radius) or at mid-diaphysis (MC3;
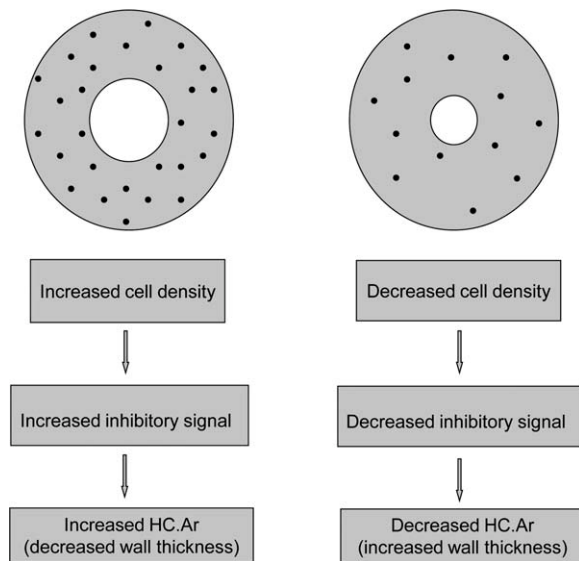
Fig. 2. Schematic representation of osteons that show the general hypothesis supported by data from Metz et al. (2003) in mature sheep ulnae. HC.Ar = Haversian canal area (=central canal area).
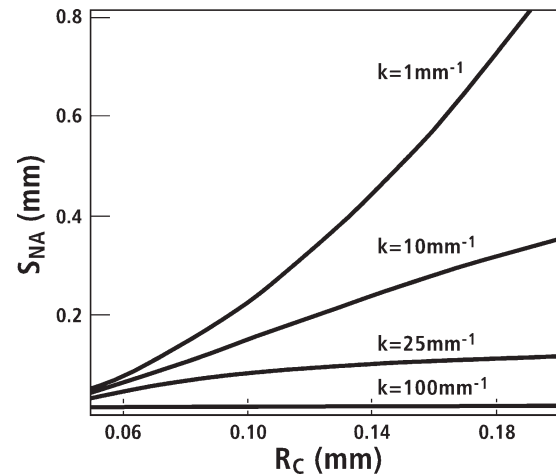

Fig. 3. The hypothesized areal inhibitory signal (normalized by volumetric signal strength), within a completed osteon, is plotted as a function of the cement line radius (R_C) for several values of the decay constant k (mm^{-1}). The radius of the HC is assumed to be 20 μm. When k surpasses about 25 mm^{-1}, the inhibitory signal on the HC plateaus as the cement line radius (R_C) exceeds 100 μm (0.10 mm on the abscissa). S_{NA} is the inhibitory signal (S_N) per unit area (subscript A) on the surface of the HC. (From Martin, Bone, 2000a, 26, 71–78, Fig. 6, © Elsevier, reproduced by permission.)

Mason et al., 1995; Skedros et al., 1996, 2005a). Each bone had been manually cleaned of soft tissue and sectioned transversely at 50% of its length (MC3), or at 50% and 65% of its length (radius), where 100% is the proximal end of the bone. One 5-mm-thick segment was cut immediately distal to these transection levels. The undecalcified, unstained segments were embedded in polymethyl methacrylate using conventional techniques (Emmanual et al., 1987), and they were subsequently ground, polished, and prepared for backscattered electron (BSE) imaging (Skedros et al., 1993).

In the MC3s, two-to-three 50× high-resolution BSE micrographs (2.3 × 1.6 mm^2) were taken within each of the three trans-cortical locations [i.e., periosteal ("outer"), middle cortical, endosteal cortex ("inner")] in quadrant locations: anterior, posterior, medial, and lateral. In the radii, two 50× (2.71 × 2.71 mm^2) BSE micrographs were taken within each of the three trans-cortical locations of the anterior "tension" and posterior "compression" cortices, and one image in each trans-cortical location of the medial and lateral ("neutral axis") cortices. The images excluded circumferential lamellar bone.

Calcanei of Horses, Elk, Sheep, and Deer

One calcaneus was obtained from each of the seven standard-bred horses with no history of racing or race training, seven wild-shot North American elk (*Cervus elaphus*), and seven domesticated sheep (*Ovis aries*, breed is crossed Suffolk/Hampshire and Rambouillet; Fig. 5). All of these bones were from adult animals that had been used in previous studies (Skedros et al., 1997, 2007b). All elk were larger males, had shed the periosteal cover of their antlers, and were obtained from their natural habitat in a fall hunting season. The horse calcanei were from mixed sexes and were not from the same animals from which the radii and MC3s were obtained. All horses were between 2 and 9 years old.

The sheep were females and ~2 years old. The sheep and horses had been kept in large pastures. Calcanei were also obtained from 10 wild-shot skeletally mature male deer used in the previous studies (Skedros et al., 1994a,b, 2007b; Skedros, 2005).

Transverse segments, 4–5-mm thick, were cut from the sheep, elk, and horse calcanei at 60% of shaft length. The deer calcanei were sectioned at both the 50% and 70% locations. These unstained, undecalcified segments were embedded in polymethyl methacrylate using conventional methods (Emmanual et al., 1987). The proximal face of each segment was ground, polished, and prepared for BSE imaging using the same techniques used for the equine radii and MC3s. One 50× BSE image representing 3.41 mm^2 (2.23 × 1.53 mm^2) was obtained in each trans-cortical location (periosteal, middle cortical, and endosteal) of the dorsal "compression" (anterior) and plantar "tension" (posterior) cortices of each specimen. Because of narrow plantar cortices of the sheep calcanei, only two images were obtained there. One image was also taken within each medial and lateral cortex ("neutral axis") of the sheep and horse calcanei. The images excluded circumferential lamellar bone.

Histomorphometric Analyses of Human Ribs

The human osteon data were obtained from archived human rib specimens that had been used by Qiu et al. (2003). These specimens had been obtained by Frost in the early 1960s from the middle portions of the fifth, sixth, or seventh ribs of nine previously healthy 20–25-year-old white male cadavers. The method of specimen processing has been previously described (Frost, 1960). In brief, 3-in. (7.6 cm) rib segments were placed in 1% basic fuchsin and 40% ethyl alcohol for 4 weeks and then immersed in a large volume of tap water for 48 hr.
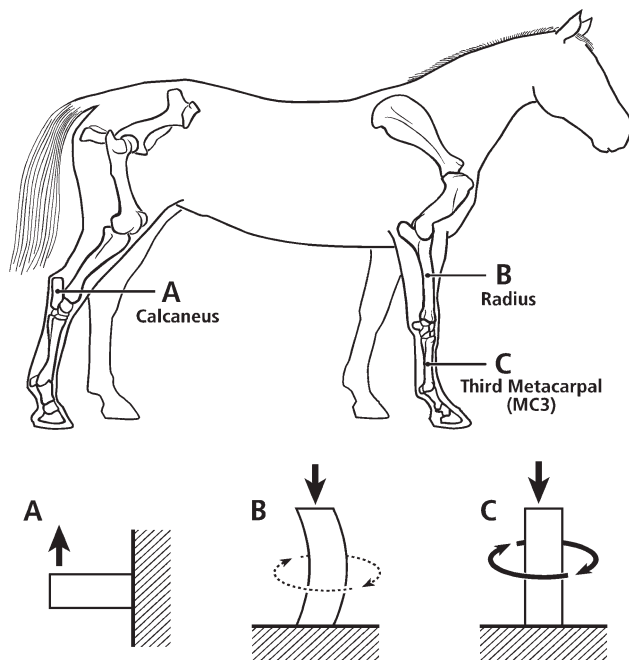
Fig. 4. Lateral-to-medial views of the right forelimb and hind-limb skeletons of an adult horse showing a spectrum from simple loading to complex loading, respectively: calcaneus (**A**), radius (**B**), and third metacarpal (MC3; **C**). The drawings below are simplified renditions of each bone type, showing (A) the calcaneus as a cantilevered beam and (B) the radius as a curved beam with longitudinal loading; the curvature accentuates bending. Torsion (dotted line) is also present but is less than the torsion in the MC3 (solid circular line in C), and (C) the MC3 with off-axis longitudinal loading producing bending and torsion, the latter being greater than in the other two bones. Several studies reporting *in vivo* strain data were used to create these drawings (Lanyon, 1974; Turner et al., 1975; Rubin and Lanyon, 1982; Schneider et al., 1982; Biewener et al., 1983a,b; Gross et al., 1992; Su et al., 1999).
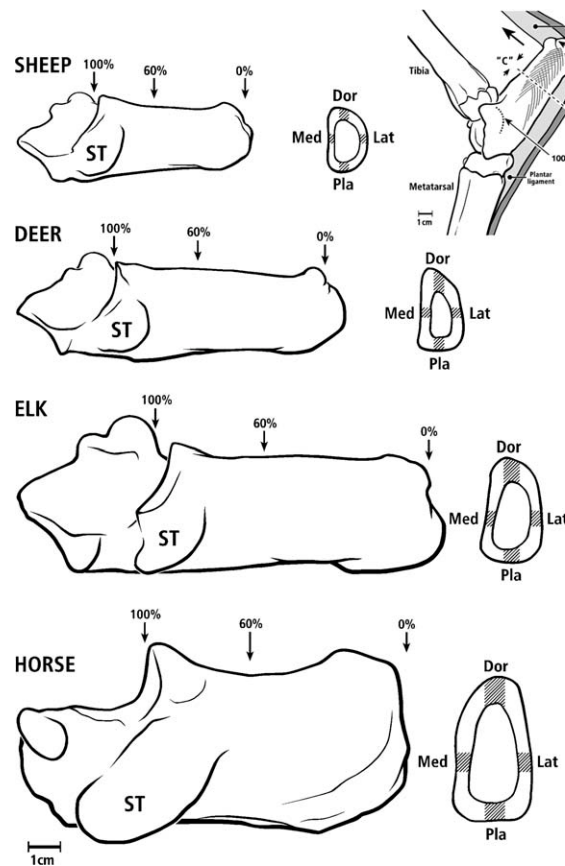

Fig. 5. All calcanei in medial-to-lateral view; from top to bottom: sheep, deer, elk, and horse. Cross-sections show image locations in gray. One section (60% location) was analyzed in sheep, elk, and horse bones, and two sections (50% and 70% locations) were analyzed in deer bones. Dor: dorsal; Pla: plantar; Med: medial; and Lat: lateral. The inset drawing at the upper right shows an adult right deer calcaneus in lateral-to-medial view showing typical loading along the Achilles tendon (large arrow) producing net compression ("C") and tension ("T") on dorsal and plantar cortices, respectively. This loading regime is similar in all of the calcanei used in this study. In this figure, the "Achilles tendon" represents the common calcaneal tendon.

After the samples were hydrated, transverse sections were cut from each rib, ground to a thickness of about 50 μm, and mounted on slides.

Microscopic analysis of the rib osteons and their osteocyte lacunae (Ot.Lc.N) was performed on the images obtained from the transverse cross-sections using a Nikon microscope with a CCD video camera (Optronics, Goleta, CA). Each microscopic image was imported to a Bioquant NOVA image analysis system (R&M Biometrics, Nashville, TN) with a panel sized 640 × 480 pixels. The length and width of the panel under 1× objective was 6.717 × 5.908 mm^2. All of the secondary osteons that met the following criteria were examined: (1) an intact osteon with a clear boundary at the cement line, (2) a HC.Ar less than one-quarter of the On.Ar, with no osteoid on its surface, (3) no Volkmann's canals crossing the osteon and no aberrant or atypical osteon variant (e.g., unusually elliptical osteon, drifting osteon, and dumbbell osteon), (4) no interference from the basic fuchsin intensity with the measurement of Ot.Lc.N, and (5) staining intensity consistent with complete mineralization, in addition to the absence of osteoid. It was important to select only mature osteons for this study because sclerostin is only produced by osteocytes that are within well-mineralized matrix (Irie et al., 2008). On the basis of these criteria, a total of 398 osteons from

the nine human subjects were measured. In the ribs, the boundaries of the osteon and the Haversian canal (HC) were traced under bright light using a 10× objective, and then the stained lacunar profiles were counted under blue-violet epifluorescent light using a 20× objective. Ot.Lc.N can be readily identified under blue-violet light due to the strong fluorescence of basic fuchsin. Because epifluorescent light penetrates <5 μm below the specimen's surface, a thin section can be assumed for counting the Ot.Lc.N even when a section is thick (~100–150 μm; Mori et al., 1997; Vashishth et al., 2000; Slyfield et al., 2009). The image analysis system was used to directly measure nearly all the osteon parameters [On.Ar, HC.Ar, and mineralized bone area of an individual osteons (B.Ar)] from the digitized images. Using these measurements and assuming circularity of the osteons, mean On.W.Th was calculated for each osteon as the difference between the outer (cement line) and HC radii (Fig. 7).
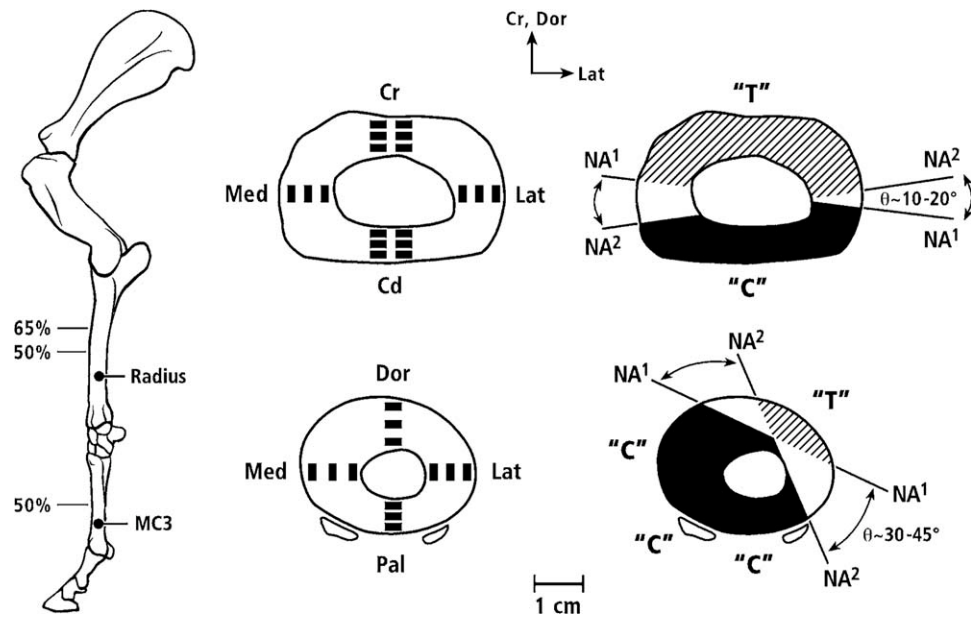
Fig. 6. Lateral-to-medial view of a left forelimb skeleton of an adult horse showing the radius and third metacarpal (MC3). At near right are the cross-sections showing image locations, and at far right are the approximate typical ranges that the neutral axes (N.A.) moves during weight bearing. Several studies reporting *in vivo* strain data were used to create these drawings (Turner et al., 1975; Rubin and Lanyon, 1982; Schneider et al., 1982; Biewener et al., 1983a,b; Gross et al., 1992). C: Compression region (darkened); T: tension region (oblique lines); Cr: cranial; Cd: caudal; Dor: dorsal; Pal: palmar; Med: medial; and Lat: lateral.
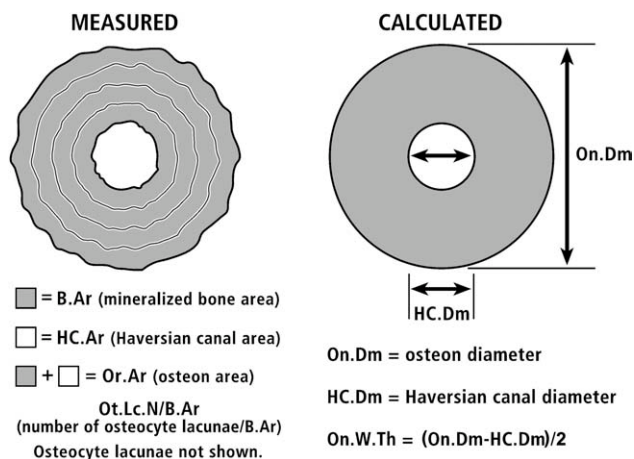

Fig. 7. **A**: Tracing of an actual osteon showing the measured parameters, which are listed below the osteon. **B**: Actual osteon converted to a perfect circle; below this drawing are the calculated parameters. Ot.Lc.N are not shown in these drawings.

Histomorphometric Analyses of Nonhuman Bones

We also evaluated complete and mature secondary osteons that had been identified in the BSE images from the transverse sections of the nonhuman limb bones in our previous studies. Maturity was determined in these images by gray levels of the osteonal walls that are indicative of complete mineralization (e.g., not relatively darker as seen in forming, or recently formed, osteons; Skedros et al., 2007a). Each nonhuman osteon was selected using the same criteria described above for the rib osteons, except for criteria #4 and #5 that involved basic fuchsin because no staining had been done on the nonhuman specimens. The Ot.Lc.N were manually counted in each osteon. Ot.Lc.N can be readily identified in the BSE images due to the stark contrasts between the black lacunae and gray bone. Furthermore, because the electrons that form the BSE images used in this study penetrate only a few microns below the specimen's surface (Skedros et al., 2005b), a thin section can be assumed for measuring Ot.Lc.N even when a bone section is thick (Bachus and Bloebaum, 1992). Using a random grid system, five osteons were selected from each image. The public domain NIH image (v.1.61) software (http://rsb.info.nih.gov/nih-image/) was used to manually trace each of the five osteons. Similar to the process used in the ribs, these tracings were converted into digitized binary images that were used to measure most of the osteon parameters. As also described above for ribs, On.W.Th was calculated as the difference between the measured outer (cement line) and HC radii (Fig. 7).

Osteon Size as a Possible Confounding Factor

To assess potential effects of osteon size on the relationship between Ot.Lc.N/B.Ar and On.W.Th, Pearson's correlation coefficients were determined for these four groups in each bone type: (1) only smaller osteons with ≤ 150 μm diameter (in ribs also: ≤ 185 μm and ≤ 200 μm, see rationale below), (2) only smaller osteons $\leq$ the mean value of the data set, (3) only the larger osteons $>$ the mean value of the data set (in ribs also: >185 μm and >200 μm), and (4) all osteons. Because of only 15 osteons in the ≤ 150 μm group of ribs, the cutoff value
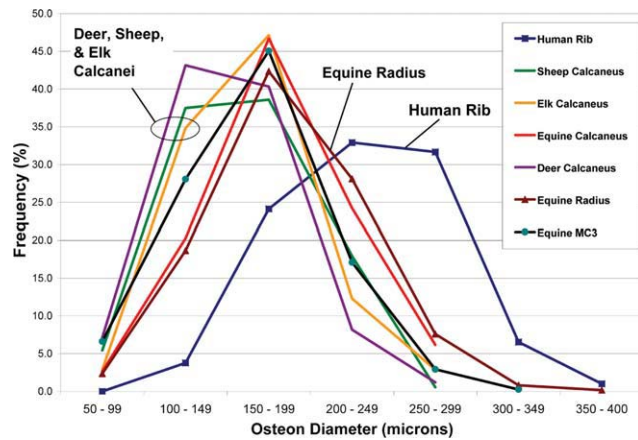
Fig. 8. Histograms of frequency distributions of the outer diameters (μm) of all osteons analyzed in this study. The outer diameter is defined by the cement line.

Fig. 9. Histograms of frequency distributions of the HC.Dm (μm) of all osteons analyzed in this study.

for this small/large osteon size distinction was raised to 185 μm (similar to the largest mean diameter value of the limb bones) and also arbitrarily to 200 μm.

The correlation coefficients in each of the four size groups were also determined for (1) comparisons of Ot.Lc.N/B.Ar with On.W.Th/On.Dm (On.Dm = osteon outer diameter), On.W.Th/On.Ar, HC.Ar/On.Ar, and B.Ar and (2) comparisons among On.W.Th, On.Dm, On.Ar, and HC.Ar.

Using a one-way analysis of variance (ANOVA) design, paired comparisons of the Ot.Lc.N/B.Ar, (Ot.Lc.N/B.Ar)/On.W.Th, (Ot.Lc.N/B.Ar)/B.Ar, Haversian canal diameter (HC.Dm), On.Dm, and HC.Dm/On.Dm were evaluated independently within each bone type between the small and large osteon groups. The parameters "(Ot.Lc.N/B.Ar)/On.W.Th" and "(Ot.Lc.N/B.Ar)/B.Ar" allowed for the assessment of influences of the calculated linear measurement of wall thickness compared with the measured wall "thickness" expressed as the area of the osteon wall (B.Ar; Fig. 7). In turn, this distinction allowed for the detection of potential influences of osteon obliquity, which would be revealed by discrepancies between these calculated and measured parameters in the paired comparison analyses (ANOVA and/or correlations). The criterion for statistical significance was $P \leq 0.05$ and variability was expressed as the standard deviation.

RESULTS

Osteon diameters (On.Dm) varied greatly (Fig. 8), and this was the dominant factor governing On.W.Th because the range of HC.Dm was much less (Fig. 9). Indeed, linear regression analysis showed that On.Dm accounted for $\geq 89\%$ of the variability in On.W.Th when all osteons were considered in each bone type. In regression analyses of small versus large osteons, On.Dm remained a dominant factor in governing On.W.Th but the variability explained was somewhat less, ranging from 67% to 89%.

Correlation analyses of On.W.Th with On.Dm and of On.W.Th with On.Ar showed consistently strong relationships that are expected between these parameters in each of the seven bone types (data not shown). By con-
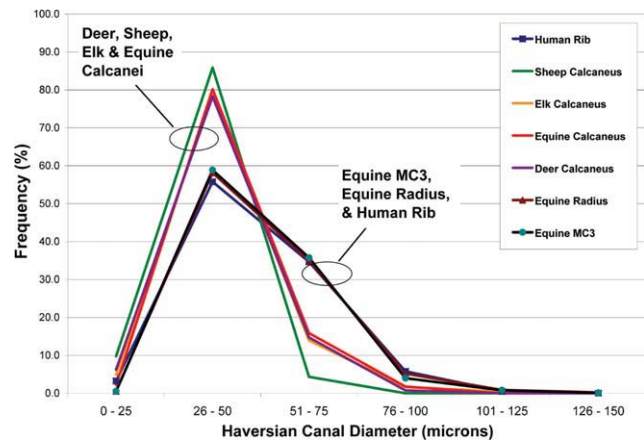
trast, positive correlations of HC.Ar with On.Ar were more variable, with the ribs showing the strongest correlation (r = 0.639 when all osteons were considered) when compared with the limb bones (range of r values in limb bones: 0.044–0.449). This reflects relatively greater increases in HC.Ar with the increases in On.Ar in the rib osteons.

Table 2 summarizes the results of correlations between Ot.Lc.N/B.Ar and On.W.Th or On.W.Th/On.Dm. In general, these results revealed correlations that, although statistically significant (i.e., significantly different from no correlation), were typically weak—the variability explained in these relationships ranged from ~2% to 22%. As described below, these results neither strongly nor consistently support the hypotheses; the elk calcanei are an obvious exception in terms of the small versus large osteon analysis.

Figure 10 shows the diagrammatic representations of 14 actual osteons that were selected from the equine radii and human ribs (seven osteons from each species). These represent the range of On.Dm from the smallest to the largest. Figure 11 shows the three representative BSE images obtained from a deer calcaneus and horse radius.

Correlations of Ot.Lc.N/B.Ar With On.W.Th

In Table 2, the first row within each bone type lists the results of correlation analyses of Ot.Lc.N/B.Ar with On.W.Th using the data from all osteons as well as data segregated by the osteon size. Each limb bone showed a significant negative correlation between Ot.Lc.N/B.Ar and On.W.Th ($P < 0.001$; r values typically -0.30 to -0.50). These results are also consistent with the magnitude of the negative correlation shown previously in the osteons of sheep ulnae (r = -0.39, $P < 0.0001$; Metz et al., 2003). Analysis of human rib data, however, showed a much weaker negative correlation (r = -0.102, $P = 0.04$).

Evaluation of Influences of Osteon Size

Results of correlation analyses in groups defined by the small (≤ 150 μm diameter; in ribs also: ≤ 185 and

TABLE 2. Correlations of Ot.Lc.N/B.Ar with On.W.Th and On.W.Th/On.Dm in small, mean-small, mean-large, and all osteons from each species[a]

Species & bone	On.Lc.N/B.Ar vs	Small osteons		Mean-small osteons[b]		Mean-large osteons[b]		All osteons	
		r	P	r	P	r	P	r	P
Sheep calcaneus		**Small, ≤150 μm**		**Small, ≤161 μm**		**Large, >161 μm**		**All**	
	On.W.Th	−0.517	<0.001	−0.498	0.001	−0.195	0.1	−0.475[c]	<0.001
	On.W.Th/On.Dm	−0.311	<0.01	−0.323	<0.01	−0.126	0.2	−0.402[c]	<0.001
Deer calcaneus		**Small, ≤150 μm**		**Small, ≤152 μm**		**Large, > 152 μm**		**All**	
	On.W.Th	−0.238	<0.001	−0.230	<0.001	−0.216	<0.001	−0.337	<0.001
	On.W.Th/On.Dm	−0.150	<0.01	−0.141	<0.01	0.060	0.3	−0.170[c]	<0.001
Elk calcaneus		**Small, ≤150 μm**		**Small, ≤164 μm**		**Large, >164 μm**		**All**	
	On.W.Th	−0.170	0.1	−0.284	<0.001	−0.260	<0.01	−0.360	<0.001
	On.W.Th/On.Dm	−0.018	0.9	−0.090	0.3	−0.099	0.3	−0.163[c]	0.01
Equine calcaneus		**Small, ≤150 μm**		**Small, ≤181 μm**		**Large, >181 μm**		**All**	
	On.W.Th	−0.475	<0.001	−0.456	<0.001	−0.080	0.4	−0.467[c]	<0.001
	On.W.Th/On.Dm	−0.380	<0.01	−0.373	<0.001	−0.102	0.3	−0.361[c]	<0.001
Equine radius		**Small, ≤150 μm**		**Small, ≤186 μm**		**Large, >186 μm**		**All**	
	On.W.Th	−0.384	<0.001	−0.403	<0.001	−0.130	<0.001	−0.386[c]	<0.001
	On.W.Th/On.Dm	−0.303	<0.001	−0.310	<0.001	−0.091	<0.01	−0.301	<0.001
Equine MC3		**Small, <150 μm**		**Small, ≤166 μm**		**Large, >166 μm**		**All**	
	On.W.Th	−0.442	<0.001	−0.430	<0.001	−0.152	<0.001	−0.419[c]	<0.001
	On.W.Th/On.Dm	−0.365	<0.001	−0.371	<0.001	−0.065	0.02	−0.340[c]	<0.001
Human rib		**Small, ≤150 μm**		**Small, ≤232 μm**		**Large, >232 μm**		**All**	
	On.W.Th	−0.285	0.3	−0.167	0.02	−0.011	0.9	−0.102[c]	0.04
	On.W.Th/On.Dm	−0.196	0.5	−0.228	<0.01	0.026	0.7	−0.110[c]	0.03
		Small, ≤185 μm		**Small, ≤200 μm**		**Large, >185 μm**		**Large, >200 μm**	
	On.W.Th	−0.453	<0.001	−0.210	0.03	−0.066	0.2	−0.025	0.7
	On.W.Th/On.Dm	−0.334	<0.01	−0.258	0.01	−0.043	0.4	−0.023	0.7

[a]r = correlation coefficient.
[b]These small vs large distinctions are based on the mean diameter of the osteons in each bone type.
[c]Cases dealing with On.W.Th or On.W.Th/On.Dm where correlation coefficients differ more than the absolute value of 0.3 and/or P values change from significant to nonsignificant (or vice versa) in the analyses of the six columns on the right side of the table [mean-small ([b]), large ([b]), or all osteons]. See text for details.

≤200 μm), mean-small (≤the mean On.Dm), and large osteon (>the mean On.Dm; in ribs: >185 and >200 μm) distinctions are summarized in Table 2. These results generally show (elk calcanei are an exception) a possible affect of osteon size on the relationship of Ot.Lc.N/B.Ar with On.W.Th or with On.W.Th/On.Dm.

Results of these small versus large osteon analyses also show that, in all cases, the absolute strengths of the correlations of Ot.Lc.N/B.Ar versus On.W.Th were greater in the mean-small osteon group than in the larger osteon group. However, as noted, this was not the case in the elk calcanei when their small osteon group was defined by the ≤150 μm diameter cutoff: (1) ≤150 μm: r = −0.170, P = 0.1 and (2) >164 μm: r = −0.260, P < 0.01.

In ribs, an effect of On.Dm is suggested by results showing that, when compared with the larger osteons, the smaller osteon groups (≤185 and ≤200 μm) exhibited increases in the strength of the correlation of Ot.Lc.N/B.Ar with On.W.Th; for example: (1) ≤185 μm: r = −0.453, P < 0.001 and (2) >185 μm: r = −0.066, P = 0.2 (Table 2).

Correlations supporting the second hypothesis (an effect of On.Dm) in most bones examined are consistent with the results of ANOVA paired comparisons. These comparisons showed that (Ot.Lc.N/B.Ar)/On.W.Th and (Ot.Lc.N/B.Ar)/B.Ar were each greater in the smaller than the larger osteon groups in all the seven bone types (P < 0.001; Table 3). In contrast to these findings, (1) the elk calcanei only showed the statistically significant

negative correlation of Ot.Lc.N/B.Ar with On.W.Th/On.Dm when all osteons are considered (i.e., the first hypothesis of the inverse relationship appears to be weakly supported, but the second hypothesis of an osteon size effect was rejected because these correlations were not significant in the small, mean-small, and large osteon groups; Table 2) and (2) the equine radii and equine MC3s showed a much weaker influence of osteon size, the correlation coefficients dealing with their large osteon groups remained negative and significant but have absolute magnitudes <0.1.

DISCUSSION

The results of this study do not provide clear or consistent support for an inverse relationship between osteocyte density and wall thickness of fully formed secondary osteons. Although this conclusion is mainly based on the correlations, which cannot directly elucidate specific mechanisms or causation, we feel that a strong relationship between osteon infilling and Ot.Lc.N/B.Ar, if present, would have been detected in the five species that were analyzed. However, this opinion reflects our initial thinking in terms of the hypothesis of Marotti and Martin that osteocytes repress infilling via signaling of a neural-like network. Alternatively, if sclerostin serves this repressive function, then it may be that the osteocytes closest to the forming central canal have the greatest effect on the osteoblasts. In other words, non-uniform concentration of sclerostin across the osteonal

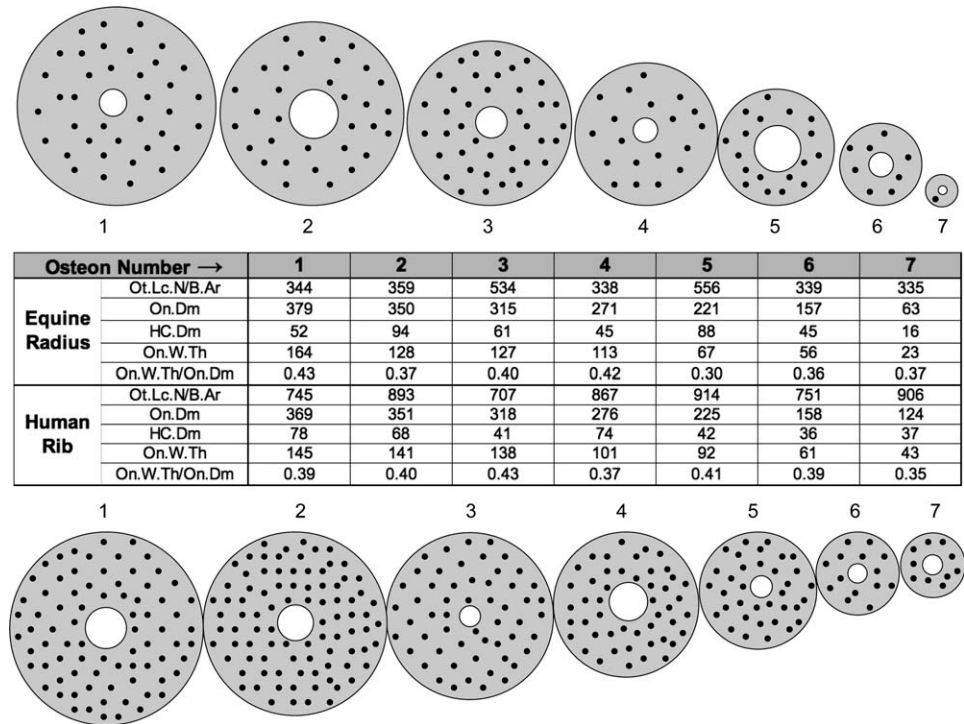| Osteon Number →		1	2	3	4	5	6	7
Equine Radius	Ot.Lc.N/B.Ar	344	359	534	338	556	339	335
	On.Dm	379	350	315	271	221	157	63
	HC.Dm	52	94	61	45	88	45	16
	On.W.Th	164	128	127	113	67	56	23
	On.W.Th/On.Dm	0.43	0.37	0.40	0.42	0.30	0.36	0.37
Human Rib	Ot.Lc.N/B.Ar	745	893	707	867	914	751	906
	On.Dm	369	351	318	276	225	158	124
	HC.Dm	78	68	41	74	42	36	37
	On.W.Th	145	141	138	101	92	61	43
	On.W.Th/On.Dm	0.39	0.40	0.43	0.37	0.41	0.39	0.35

Fig. 10. Depicted are the diagrams based on the seven osteons from the equine radii (at top) and seven osteons from the human ribs (at bottom). They range from the smallest to largest On.Dm. The intervening osteons are also the depictions of actual osteons spaced at approximately equal intervals of diameters from this range. The osteons are drawn to scale with contours that are smoothed to make them circular; the distribution of osteocytes are shown to be quasi random for illustrative purposes. The chart in the center lists the actual data for each osteon (1, 2, 3, ..., 7). Ot.Lc.N/B.Ar = no./mm^2 and other nonratio values are in micrometers.

wall (e.g., highest near the central canal) might be seen as a weak relationship in Ot.Lc.N/B.Ar versus On.W.Th/On.Dm, when linear correlations that are used to indirectly detect this effect are based on the osteocyte density data from the entire osteon wall. The strengths of the correlations could also be influenced by an unrecognized effect of variations in osteocyte density from the outer margin of the osteon toward the central canal. In a recent study using ultra-high-resolution micro-computerized tomography (Synchotron) to image human secondary osteons (11 osteons; lateral aspect of proximal femoral cortex; 25-year-old male), Hannah et al. (2010) show a clear trend of decreased numbers of osteocytic lacunae toward the central canal. If this trend is also present in the osteons examined in our study, it could play a role in diminishing the strength of the correlations. Experimental data have also shown that convective fluid flow can produce nonuniform concentrations of proteins and other molecules that have the capacity to be moved/transported through the interstitial micro-porosities of bone (Knothe Tate et al., 1998). In this perspective, it seems plausible that the repressive effect of a protein like sclerostin could be present, even though little or no correlation is detected between an osteon's osteocyte density and wall thickness.

There are additional complexities in cellular dynamics that can influence the process of osteon infilling and thereby obscure "expected" correlations of osteocyte density with wall thickness. For example, intercellular gap-junction communication is another way that osteocytes can communicate with osteoblasts and potentially modulate their responses to mechanical signals (Taylor et al., 2007). Osteoblast apoptosis may also be a factor that influences the termination of bone formation during osteon infilling (Parfitt, 1994; Qiu et al., 2010). Several studies have additionally demonstrated the spatial relationship between osteocyte apoptosis and osteoclastic bone resorption (Aguirre et al., 2006; Hedgecock et al., 2007; Emerton et al., 2010), but the causal molecular or signaling link has not yet been identified between these two processes. The osteocyte has been thought to reduce osteoclastic bone resorption by secreting antiresorptive molecules (Gu et al., 2005). The death of osteocytes causes the loss of these antiresorptive molecules, facilitating osteoclast precursor recruitment, osteoclastogenesis, and bone resorption (Gu et al., 2005). In addition, Kogianni et al. (2008) reported that apoptotic osteocytes could release signals, such as tumor necrosis factor-alpha (TNF-α), to initiate osteoclastogenesis and subsequent bone resorption. Osteoclasts, in turn, establish the size of the resorption space (i.e., the On.Dm), which cannot be larger than what the central capillary can supply to the tissue of the osteon wall (Ham, 1952). Clearly, much remains to be learned about how cellular and other biophysical factors interact in the regulation of osteon infilling.

Additional issues dealing with cell viability and age-related degradations in normal cell function point out what may be an important limitation of our study—we were not able to quantify the percentage of viable cells in the osteocytic lacunae. It could be that a greater
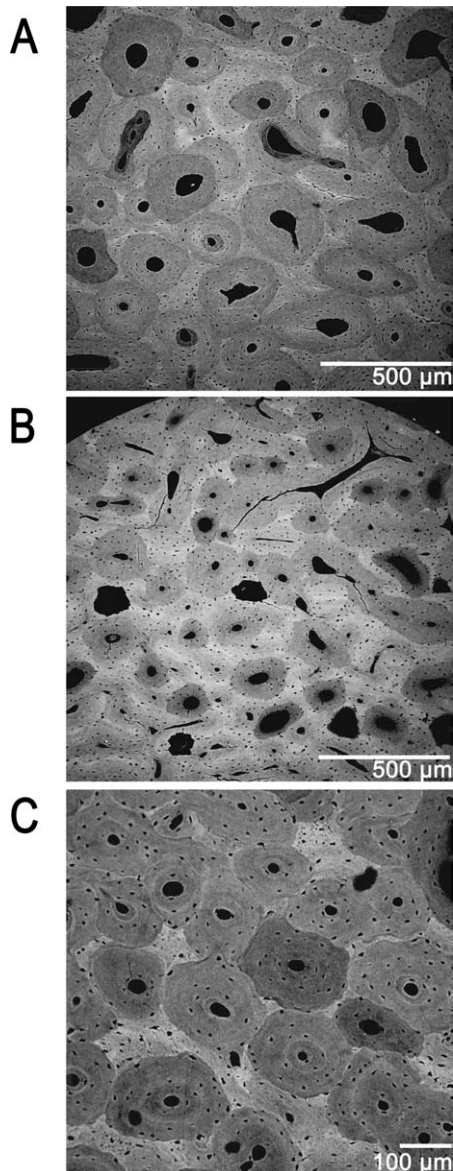
Fig. 11.   Three representative BSE images showing osteon size variations in (**A**) equine radius, caudal cortex at 100×; (**B,C**) deer calcaneus, plantar cortex at 50× (B) and 100× (C). The counting of Ot.Lc.N in the 50× BSE images used in this study was facilitated with the aid of a magnifying lens.

lacunae regardless of whether they contained evidence of a cell body. Facts supporting the probability that our bones had relatively smaller percentages of empty lacunae include (1) studies of osteocyte viability in younger individuals, such as those examined in most of the bones in our study (the elk could be an exception, discussed below), show small percentages of empty lacunae (Qiu et al., 2006) and (2) we did not observe regions with lacunae that were plugged with hypermineralized tissue that has been associated with aging, ischemia, or necrosis (Frost, 1960; Currey, 1964; Kornblum and Kelly, 1964; Jowsey, 1966; Parfitt, 1993). These observations and the younger ages of the humans and most of the animals used in our study suggest that the percentage of dead osteocytes is small. In the nonhuman bones, this is also consistent with the observations of >90% lacuna occupancy in the dorsal cortex of MC3s from thoroughbred and quarter horses with ages that are similar to the horses used in the present study (Da Costa Gomez et al., 2005; Dr. Peter Muir, personal communication). Furthermore, the imaging methods used in our study are sufficiently sensitive to detect the presence of micropetrosis because of the obvious hypermineralized material that occludes the Ot.Lc.N in this condition (Busse et al., 2010). This phenomenon was not seen in any of the images, and it would also be unexpected because the relatively younger age of the humans and of a majority of the animals that we studied.

Another possible limitation of the present study is the fact that osteon circularity was assumed in the steps that were taken to calculate the wall thickness from the measured On.Ar and HC.Ar (Fig. 7). In a perfect circle, the diameter will have a very strong correlation with the area [since area $= \pi (1/2 Dm)^2$]. The difference between correlations of Ot.Lc.N/B.Ar with On.W.Th/On.Dm when compared with Ot.Lc.N/B.Ar with On.W.Th/On.Ar suggests that there is some obliquity to the osteons. We attempted to minimize this variable [as did Metz et al. (2003)] by avoiding the analysis of obviously elliptical or otherwise unusual osteon variants. These exclusion criteria were deemed reasonable because these atypical osteon morphologies represent a minority of the osteons in the images used in the present study (Skedros et al., 2007b).

Given the small size of Ot.Lc.N, the sampling volume of microscopic techniques could be an important confounding factor in a two-dimensional analysis. This might seem to be an important consideration for the present study because two different microscopic techniques were used: epifluorescent microscopy was used to analyze the human ribs and BSE microscopy was used to analyze the nonhuman bones. However, the sampling volumes of each technique do not extend beyond the breadth of a typical osteocyte lacuna (Canè et al., 1982; Hannah et al., 2010). For the epifluorescent technique, this was assured by the use of blue-violet light because it penetrates only the first few microns of the bone section, allowing Ot.Lc.N to be quantified without projection due to section thickness (Mori et al., 1997; Vashishth et al., 2000; Slyfield et al., 2009). A confounding effect of section thickness is also eliminated in BSE imaging because only a few microns of the bone surface are sampled when using the electron beam parameters used in this study (Bachus and Bloebaum, 1992; Skedros et al., 2005b).

percentage of osteocytes were alive/functional in the small osteons compared with the large osteons, thus explaining the differences between large and small osteon responses. Unfortunately, it was not possible to ascertain osteocyte viability in our slides. However, by counting lacunae irrespective of their contents, our intent was to understand the role of osteocytes in controlling osteoblasts during osteonal infilling; we were interested in osteocyte density as it was originally during the formation of the fully formed osteons that were quantified. Therefore, assuming that each osteocyte lacuna had originally contained a living cell during osteon formation, we counted [as did Metz et al. (2003)] all

TABLE 3. ANOVAs and descriptive statistics (means and standard deviations)

Species & bone	Osteon size[a]	Ot.Lc.N/B.Ar (no./mm²)	(Ot.Lc.N/B.Ar)/On.W.Th	(Ot.Lc.N/B.Ar)/B.Ar	HC.Dm (μm)	On.Dm (μm)	HC.Dm/On.Dm
Sheep calcaneus	Small osteons (≤161 μm, n = 97)	756 ± (265)	17,210 ± (11,613)	74,487 ± (70,378)	32 ± (8)	131 ± (21)	0.25 ± (0.07)
	Large osteons (>161 μm, n = 87)	599 ± (154)	7,620 ± (2,413)	21,896 ± (8,112)	33 ± (8)	195 ± (23)	0.17 ± (0.05)
	All osteons	683 ± (232)	12,675 ± (9,825)	49,621 ± (57,641)	32 ± (8)	161 ± (39)	0.21 ± (0.07)
Deer calcaneus	Small osteons (≤152 μm, n = 349)	695 ± (253)	17,372 ± (12,859)	75,898 ± (87,217)	36 ± (10)	125 ± (20)	0.29 ± (0.09)
	Large osteons (>152 μm, n = 343)	575 ± (172)	8,429 ± (3,099)	24,961 ± (10,493)	41 ± (13)	182 ± (26)	0.22 ± (0.07)
	All osteons	637 ± (226)	13,074 ± (10,505)	51,415 ± (68,166)	38 ± (12)	152 ± (37)	0.26 ± (0.09)
Elk calcaneus	Small osteons (≤164 μm, n = 136)	750 ± (217)	15,906 ± (7,143)	61,584 ± (37,991)	37 ± (10)	137 ± (20)	0.27 ± (0.08)
	Large osteons (>164 μm, n = 108)	649 ± (136)	8,856 ± (2,657)	24,150 ± (8,252)	44 ± (15)	197 ± (23)	0.23 ± (0.04)
	All osteons	705 ± (192)	12,786 ± (6,616)	45,015 ± (34,336)	40 ± (12)	163 ± (37)	0.25 ± (0.08)
Equine calcaneus	Small osteons (≤181 μm, n = 111)	692 ± (192)	13,647 ± (6,956)	51,478 ± (37,694)	37 ± (8)	147 ± (23)	0.25 ± (0.06)
	Large osteons (>181 μ m, n = 116)	553 ± (126)	6,715 ± (1,856)	16,931 ± (5,560)	45 ± (13)	214 ± (27)	0.21 ± (0.06)
	All osteons	622 ± (175)	10,104 ± (6,112)	33,824 ± (31,731)	41 ± (12)	181 ± (42)	0.23 ± (0.06)
Equine radius	Small osteons (≤186 μm, n = 1,200)	520 ± (206)	11,118 ± (8,358)	40,760 ± (45,159)	45 ± (11)	151 ± (26)	0.30 ± (0.08)
	Large osteons (>186 μm, n = 1,144)	419 ± (128)	5,164 ± (1,950)	12,146 ± (5,154)	55 ± (17)	224 ± (31)	0.25 ± (0.07)
	All osteons	471 ± (180)	8,212 ± (6,817)	26,795 ± (35,514)	50 ± (15)	186 ± (46)	0.28 ± (0.08)
Equine MC3	Small osteons (≤166 μm, n = 1,223)	644 ± (297)	19,637 ± (25,810)	76,257 ± (107,414)	47 ± (12)	132 ± (25)	0.36 ± (0.01)
	Large osteons (> 166 μm, n = 1,235)	496 ± (148)	7,101 ± (2,841)	18,460 ± (8,019)	53 ± (16)	199 ± (27)	0.27 ± (0.08)
	All osteons	570 ± (246)	13,338 ± (19,357)	47,217 ± (81,278)	50 ± (11)	166 ± (43)	0.32 ± (0.11)
Human rib	Small osteons (≤200 μm, n = 111)	865 ± (138)	13,087 ± (3,376)	40,744 ± (14,166)	37 ± (10)	173 ± (19)	0.22 ± (0.06)
	Large osteons (>200 μm, n = 287)	842 ± (125)	8,493 ± (1,780)	18,125 ± (5,468)	53 ± (14)	256 ± (34)	0.21 ± (0.05)
	Small osteons (≤232 μm, n = 191)	856 ± (135)	11,741 ± (3,230)	33,793 ± (13,831)	40 ± (10)	191 ± (27)	0.21 ± (0.05)
	Large osteons (>232 μm, n = 207)	841 ± (123)	7,960 ± (1,474)	15,796 ± (3,853)	57 ± (14)	271 ± (28)	0.21 ± (0.05)
	All osteons	848 ± (129)	9,775 ± (3,114)	24,433 ± (13,428)	49 ± (15)	232 ± (48)	0.21 ± (0.05)

▨ = Grayed cells indicate statistically significant differences ($P \leq 0.05$) between large and small osteons in the same column and within the bone type.
[a]Small osteons in this column are based on the mean diameter in each bone type; a 200 μm cutoff is also shown for the ribs. Large osteons are defined as greater than the mean diameter of the osteons in each bone type.

Clearly, several factors influence osteon morphology, including one of the dominant variables demonstrated in this study—On.Dm. The influence of On.Dm and the rather weak correlations shown herein could be considered in terms of Martin's (2000a) caution that an osteocyte-network inhibitory signal at the HC surface would be very sensitive to the efficiency with which it can be passed from one osteocyte to another (Fig. 3). Spatial signal decay/plateau may help to explain our results showing that correlations of Ot.Lc.N/B.Ar with On.W.Th/On.Dm were significant in the smaller osteons (in all but elk calcanei; discussed further below) but became nonsignificant in osteons with diameters greater than ~150–190 μm. Alternatively, as mentioned above, these data could be explained by spatial variations in the efficiency of a signaling protein that is "transported" through the microporosities of bone matrix and/or by other unrecognized complexities of cellular regulation of infilling.

In addition to the "transport" of sclerostin toward osteoblasts, the dynamics of nutrient delivery during osteon infilling must be considered in the perspective of the differences shown in the present study between smaller and larger osteons. For example, if during the earlier phase of infilling, the outermost osteocytes of smaller osteons more quickly become nutrient deficient when compared with the outermost portions of larger osteons [i.e., greater HC surface area for nutrient exchange in larger osteons], then the relative degree of "starvation" of the outermost osteocytes may be relatively greater in smaller osteons during their initial infilling. If this occurs, then the inhibitory signal might influence the duration of infilling and/or the formation period differently between these groups. If correct, this might help explain our data showing that the HC.Dm/On.Dm ratio is greatest in the smaller osteon group ($P < 0.05$) in all of the limb bones. This suggests that the hypothesized inhibitory signal is relatively deficient and/or becomes less precise in larger osteons. To test this hypothesis, additional studies of the dynamics of osteon formation are needed to evaluate potential differences in appositional rates, osteocyte densities, temporal/spatial variations in sclerostin concentration, and formation periods between early, middle, and late infilling phases of osteons from a broad size range.

In addition to considering the possibility that osteocyte repression influences the extent of osteon infilling, an independent effect of infilling rate on osteocyte density should be considered. On.Dm might also be important in this context, because relatively faster rates of osteon infilling have been shown in larger versus smaller osteons in dog ribs (r = 0.52; Ilnicki et al., 1966), dog limb bones (e.g., femur; r = 0.87; Lee, 1964), rabbit limb bones (Jee and Arnold, 1954), and human limb and rib bones (Polig and Jee, 1990). In turn, data from sheep ulnae reported by Metz et al. (2003) support the possibility that infilling rate, expressed as mineral appositional rate (MAR), is positively correlated with osteocyte density. Though statistically significant, this effect was weak as shown by the correlation between Ot.Lc.N/B.Ar and normalized intracortical MAR ($r^2 = 0.12$, $P = 0.0001$). Taken together, these data might suggest that the density of osteocytes remaining after osteonal infilling is, at best, weakly influenced by the positive relationship between MAR and osteon size. However, a recent rigorous study of the relationships of modeling and remodeling with osteocyte density and apoptosis in rabbit tibia mid-shafts did not find significant relationships between osteocyte lacuna or osteocyte densities and intracortical (osteonal) or surface bone formation rates (Hedgecock et al., 2007). In this perspective, it seems unlikely that the osteocyte density differences shown in the present study are strongly influenced by the relationship between MAR and On.Dm.

Results in elk calcanei showing no correlations in small or large osteons (Ot.Lc.N/B.Ar vs. On.W.Th or On.W.Th/On.Dm) are anomalous in view of the correlations shown consistently (although weak) among these parameters in the smaller osteons in the other six bone types. This exception could reflect a flaw in the hypothesis that osteon infilling is regulated, to some extent, by osteocyte density. This possibility can only be resolved by the additional experimental studies that control for factors that are not apparent in the present study. For example, in our sample of elk calcanei, it is possible that there is a significant influence of aging on osteon infilling dynamics, which has been described in the other species (e.g., decreasing osteon size with age; Lee, 1964; Ilnicki et al., 1966; Pirok et al., 1966; Britz et al., 2009). This possibility is consistent with our elk being larger/older bulls, reflecting the fact that elk hunters are typically interested in shooting trophy-sized animals. Consequently, among all of the animals studied, the elk might have been, in general, relatively older in terms of their typical life expectancy. Additionally, data in adult human femora show that osteon diameter is inversely related to body weight (Britz et al., 2009). These data support the idea that osteons (and remodeling processes) are dictated (to some degree) by load bearing or "usage." Perhaps the apparently anomalous results in the elk bones could be due to the fact that these are quite large animals, older, and very active compared with the other bones.

The fact that the ribs showed the weakest correlations of Ot.Lc.N/B.Ar with On.W.Th or On.W.Th/On.Dm (all osteons considered) might reflect important species differences in osteocyte/osteon physiology and morphology or could reflect the fundamental differences in these contexts between ribs and limb bones. There are data supporting the possibility of significant differences in mechanosensitivity between osteocytes of the axial (e.g., ribs and calvarium) and osteocytes of the appendicular (limb) skeleton (Raab et al., 1991; Tommerup et al., 1993; Rawlinson et al., 1995; Vatsa et al., 2008). In this perspective, the thresholds for metabolic activity of bone cells in ribs are probably fundamentally different when compared with the appendicular bones—ribs are more sensitive to hormonal changes associated with lactation and other highly mineral-dependent demands, while appendicular bones are less so (Vajda et al., 1999). In fact, expression of sclerostin is regulated by both mechanical stimulation and PTH, suggesting that both mechanical and metabolic influences may signal through osteocytes to inhibit bone formation by osteoblasts on the surface of the bone (Bellido et al., 2005; Robling et al., 2008; Sims and Gooi, 2008). Consequently, in some species or circumstances, metabolic demands could be sufficient to affect osteonal morphology and biomechanics differently in ribs when compared with the limb bones. These considerations might prove helpful in

explaining why in this study the osteons of the ribs, compared with the osteons of limb bones, are generally relatively larger, have higher numbers of Ot.Lc.N, have similar HC.Dm/On.Dm ratios in small and large osteons, and exhibit relatively lower correlations of Ot.Lc.N/B.Ar with On.W.Th/On.Dm (Table 2 and Fig. 10). Although the results of computational analyses and some histomorphometric studies of various limb bones show inverse relationships between mechanical stress and On.Dm (i.e., higher stress produces smaller osteons; van Oers et al., 2008; Britz et al., 2009), anthropological studies of osteon cross-sectional dimensions from rib and femora of the same individuals show that rib osteons are not consistently larger (Pfeiffer et al., 2006).

In summary, the results of this study do not provide clear or consistent support for the hypothesized inverse relationship between osteocyte density and wall thickness of fully formed secondary osteons. However, linear correlation analyses could fail to detect this evidence, although indirect, of osteocyte-based repression of osteon infilling if the signal is spatially nonuniform (e.g., increased near the central canal).

ACKNOWLEDGEMENTS

LITERATURE CITED

Aguirre JI, Plotkin LI, Stewart SA, Weinstein RS, Parfitt AM, Manolagas SC, Bellido T. 2006. Osteocyte apoptosis is induced by weightlessness in mice and precedes osteoclast recruitment and bone loss. J Bone Miner Res 21:605–615.

Bachus KN, Bloebaum RD. 1992. Projection effect errors in biomaterials and bone research. Cells Mater 2:347–355.

Bellido T, Ali AA, Gubrij I, Plotkin LI, Fu Q, O'Brien CA, Manolagas SC, Jilka RL. 2005. Chronic elevation of parathyroid hormone in mice reduces expression of sclerostin by osteocytes: a novel mechanism for hormonal control of osteoblastogenesis. Endocrinology 146:4577–4583.

Biewener AA, Thomason J, Goodship A, Lanyon LE. 1983a. Bone stress in the horse forelimb during locomotion at different gaits: a comparison of two experimental methods. J Biomech 16:565–576.

Biewener AA, Thomason J, Lanyon LE. 1983b. Mechanics of locomotion and jumping in the forelimb of the horse (*Equus*): *in vivo* stress developed in the radius and metacarpus. J Zool Lond 201:67–82.

Britz HM, Thomas CD, Clement JG, Cooper DM. 2009. The relation of femoral osteon geometry to age, sex, height and weight. Bone 45:77–83.

Burger EH, Klein-Nulend J. 1999. Mechanotransduction in bone—role of the lacunocanalicular network. FASEB J 13:S101–S112.

Busse B, Djonic D, Milovanovic P, Hahn M, Püschel K, Ritchie RO, Djuric M, Amling M. 2010. Decrease in the osteocyte lacunar density accompanied by hypermineralized lacunar occlusion reveals failure and delay of remodeling in aged human bone. Aging Cell 9:1065–1075.

Canè V, Marotti G, Volpi G, Zaffe D, Palazzini S, Remaggi F, Muglia MA. 1982. Size and density of osteocyte lacunae in different regions of long bones. Calcif Tissue Int 34:558–563.

Cooper D, Thomason C, Clement J, Hallgrimsson B. 2006. Three-dimensional microcomputed tomography imaging of basic multicellular unit-related resorption spaces in human cortical bone. Anat Rec A: Discov Mol Cell Evol Biol 288:806–816.

Currey JD. 1964. Some effects of aging in human Haversian systems. J Anat Lond 98:69–75.

Da Costa Gomez TM, Barrett JG, Sample SJ, Radtke CL, Kalscheur VL, Lu Y, Markel MD, Santschi EM, Scollay MC, Muir P. 2005. Up-regulation of site-specific remodeling without accumulation of microcracking and loss of osteocytes. Bone 37:16–24.

Emerton KB, Hu B, Woo AA, Sinofsky A, Hernandez C, Majeska RJ, Jepsen KJ, Schaffler MB. 2010. Osteocyte apoptosis and control of bone resorption following ovariectomy in mice. Bone 46:577–583.

Emmanual J, Hornbeck C, Bloebaum RD. 1987. A polymethyl methacrylate method for large specimens of mineralized bone with implants. Stain Technol 62:401–410.

Frost HM. 1960. *In vivo* osteocyte death. Am J Orthop 42-A:138–143.

Frost HM. 1990. Skeletal structural adaptations to mechanical usage (SATMU). 2. Redefining Wolff's law: the remodeling problem. Anat Rec 226:414–422.

Frost HM. 2001. From Wolff's law to the Utah paradigm: insights about bone physiology and its clinical applications. Anat Rec 262:398–419.

Gross TS, McLeod KJ, Rubin CT. 1992. Characterizing bone strain distribution *in vivo* using three triple rosette strain gauges. J Biomech 25:1081–1087.

Gu G, Mulari M, Peng Z, Hentunen TA, Vaananen HK. 2005. Death of osteocytes turns off the inhibition of osteoclasts and triggers local bone resorption. Biochem Biophys Res Commun 335:1095–1101.

Ham AW. 1952. Some histophysiological problems peculiar to calcified tissues. J Bone Joint Surg Am 24-A-3:701–728.

Hannah KM, Thomas CD, Clement JG, De Carlo F, Peele AG. 2010. Bimodal distribution of osteocyte lacunar size in the human femoral cortex as revealed by micro-CT. Bone 47:866–871.

Hedgecock NL, Hadi T, Chen AA, Curtiss SB, Martin RB, Hazelwood SJ. 2007. Quantitative regional associations between remodeling, modeling, and osteocyte apoptosis and density in rabbit tibial midshafts. Bone 40:627–637.

Herman BC, Cardoso L, Majeska RJ, Jepsen KJ, Schaffler MB. 2010. Activation of bone remodeling after fatigue: differential response to linear microcracks and diffuse damage. Bone 47:766–772.

Ilnicki L, Epker BN, Frost HM, Hattner R. 1966. The radial rate of osteon closure evaluated by means of in vivo tetracycline labeling in beagle dog rib. J Lab Clin Med 67:447–454.

Irie K, Ejiri S, Sakakura Y, Shibui T, Yajima T. 2008. Matrix mineralization as a trigger for osteocyte maturation. J Histochem Cytochem 56:561–567.

Jee WS, Arnold JS. 1954. Rate of individual Haversian system formation. Anat Rec 118:315.

Jowsey J. 1966. Studies of Haversian systems in man and some animals. J Anat 100:857–864.

Knothe Tate ML, Niederer P, Knothe U. 1998. In vivo tracer transport through the lacunocanalicular system of rat bone in an environment devoid of mechanical loading. Bone 22:107–117.

Kogianni G, Mann V, Noble BS. 2008. Apoptotic bodies convey activity capable of initiating osteoclastogenesis and localized bone destruction. J Bone Miner Res 23:915–927.

Kornblum SS, Kelly PJ. 1964. The lacunae and Haversian canals in tibial cortical bone from ischemic and non-ischemic limbs. A comparative microradiographic study. J Bone Joint Surg Am 46:797–810.

Lanyon LE. 1974. Experimental support for the trajectorial theory of bone structure. J Bone Joint Surg 56B:160–166.

Lee WR. 1964. Appositional bone formation in canine bone: a quantitative microscopic study using tetracycline markers. J Anat 98:665–677.

Marotti G. 1996. The structure of bone tissues and the cellular control of their deposition. Ital J Anat Embryol 101:25–79.

Marotti G, Ferretti M, Muglia MA, Palumbo C, Palazzini S. 1992. A quantitative evaluation of osteoblast–osteocyte relationships on growing endosteal surface of rabbit tibiae. Bone 13:363–368.

Martin RB. 2000a. Does osteocyte formation cause the nonlinear refilling of osteons. Bone 26:71–78.

Martin RB. 2000b. Toward a unifying theory of bone remodeling. Bone 26:1–6.

Mason MW, Skedros JG, Bloebaum RD. 1995. Evidence of strain-mode-related cortical adaptation in the diaphysis of the horse radius. Bone 17:229–237.

Metz LN, Martin RB, Turner AS. 2003. Histomorphometric analysis of the effects of osteocyte density on osteonal morphology and remodeling. Bone 33:753–759.

Mori S, Harruff R, Ambrosius W, Burr DB. 1997. Trabecular bone volume and microdamage accumulation in the femoral heads of women with and without femoral neck fractures. Bone 21:521–526.

Parfitt AM. 1983. The physiologic and clinical significance of bone histomorphometric data. In: Recker RR, editor. Bone histomorphometry: techniques and interpretation. Boca Raton: CRC Press, Inc. p 143–224.

Parfitt AM. 1993. Bone age, mineral density, and fatigue damage. Calcif Tissue Int 53 (Suppl 1):S82–S85; discussion S85–S86.

Parfitt AM. 1994. Osteonal and hemi-osteonal remodeling: the spatial and temporal framework for signal traffic in adult human bone. J Cell Biochem 55:273–286.

Pfeiffer S, Crowder C, Harrington L, Brown M. 2006. Secondary osteons and Haversian canal dimensions as behavioral indicators. Am J Phys Anthropol 131:460–468.

Pirok DJ, Ramser JR, Takahashi H, Villanueva AR, Frost HM. 1966. Normal histological, tetracycline and dynamic parameters in human, mineralized bone sections. Henry Ford Hosp Med J 14:195–218.

Polig E, Jee WS. 1990. A model of osteon closure in cortical bone. Calcif Tissue Int 47:261–269.

Power J, Loveridge N, Rushton N, Parker M, Reeve J. 2002. Osteocyte density in aging subjects is enhanced in bone adjacent to remodeling Haversian systems. Bone 30:859–865.

Power J, Noble BS, Loveridge N, Bell KL, Rushton N, Reeve J. 2001. Osteocyte lacunar occupancy in the femoral neck cortex: an association with cortical remodeling in hip fracture cases and controls. Calcif Tissue Int 69:13–19.

Qiu S, Fyhrie DP, Palnitkar S, Rao DS. 2003. Histomorphometric assessment of Haversian canal and osteocyte lacunae in different-sized osteons in human rib. Anat Rec 272A:520–525.

Qiu S, Rao DS, Palnitkar S, Parfitt AM. 2006. Differences in osteocyte and lacunar density between Black and White American women. Bone 38:130–135.

Qiu S, Rao DS, Palnitkar S, Parfitt AM. 2010. Dependence of bone yield (volume of bone formed per unit of cement surface area) on resorption cavity size during osteonal remodeling in human rib: implications for osteoblast function and the pathogenesis of age-related bone loss. J Bone Miner Res 25:423–430.

Raab DM, Crenshaw TD, Kimmel DB, Smith EL. 1991. A histomorphometric study of cortical bone activity during increased weight-bearing exercise. J Bone Miner Res 6:741–749.

Rawlinson SD, Mosley JR, Suswillo RF, Pitsillides AA, Lanyon LE. 1995. Calvarial and limb bone cells in organ and monolayer culture do not show the same early response to dynamic mechanical strains. J Bone Miner Res 10:1225–1232.

Riddle RC, Donahue HJ. 2009. From streaming-potentials to shear stress: 25 years of bone cell mechanotransduction. J Orthop Res 27:143–149.

Robling AG, Niziolek PJ, Baldridge LA, Condon KW, Allen MR, Alam I, Mantila SM, Gluhak-Heinrich J, Bellido TM, Harris SE, Turner CH. 2008. Mechanical stimulation of bone in vivo reduces osteocyte expression of Sost/sclerostin. J Biol Chem 283:5866–5875.

Rubin CT, Lanyon LE. 1982. Limb mechanics as a function of speed and gait: a study of functional strains in the radius and tibia of horse and dog. J Exp Biol 101:187–211.

Schneider RK, Milne DW, Gabel AA, Groom JJ, Bramlage LR. 1982. Multidirectional in vivo strain analysis of the equine radius and tibia during dynamic loading with and without a cast. Am J Vet Res 43:1541–1550.

Sims NA, Gooi JH. 2008. Bone remodeling: multiple cellular interactions required for the coupling of bone formation and resorption. Semin Cell Dev Biol 19:444–451.

Skedros JG. 2005. Osteocyte lacuna population densities in sheep, elk and horse calcanei. Cells Tissues Organs 181:23–37.

Skedros JG, Bloebaum RD, Bachus KN, Boyce TM, Constantz B. 1993. Influence of mineral content and composition of gray levels in backscattered electron images of bone. J Biomed Mater Res 27:57–64.

Skedros JG, Bloebaum RD, Mason MW, Bramble DM. 1994a. Analysis of a tension/compression skeletal system: possible strain-specific differences in the hierarchical organization of bone. Anat Rec 239:396–404.

Skedros JG, Grunander TR, Hamrick MW. 2005a. Spatial distribution of osteocyte lacunae in equine radii and third metacarpals: considerations for cellular communication, microdamage detection and metabolism. Cells Tissues Organs 180:215–236.

Skedros JG, Holmes JL, Vajda EG, Bloebaum RD. 2005b. Cement lines of secondary osteons in human bone are not mineral-deficient: new data in a historical perspective. Anat Rec A: Discov Mol Cell Evol Biol 286:781–803.

Skedros JG, Mason MW, Bloebaum RD. 1994b. Differences in osteonal micromorphology between tensile and compressive cortices of a bending skeletal system: indications of potential strain-specific differences in bone microstructure. Anat Rec 239:405–413.

Skedros JG, Mason MW, Nelson MC, Bloebaum RD. 1996. Evidence of structural and material adaptation to specific strain features in cortical bone. Anat Rec 246:47–63.

Skedros JG, Sorenson SM, Hunt KJ, Holyoak JD. 2007a. Ontogenetic structural and material variations in ovine calcanei: a model for interpreting bone adaptation. Anat Rec 290:284–300.

Skedros JG, Sorenson SM, Jenson NH. 2007b. Are distributions of secondary osteon variants useful for interpreting load history in mammalian bones? Cells Tissues Organs 185:285–307.

Skedros JG, Su SC, Bloebaum RD. 1997. Biomechanical implications of mineral content and microstructural variations in cortical bone of horse, elk, and sheep calcanei. Anat Rec 249:297–316.

Slyfield CR, Jr., Niemeyer KE, Tkachenko EV, Tomlinson RE, Steyer GG, Patthanacharoenphon CG, Kazakia GJ, Wilson DL, Hernandez CJ. 2009. Three-dimensional surface texture visualization of bone tissue through epifluorescence-based serial block face imaging. J Microsc 236:52–59.

Su SC, Skedros JG, Bachus KN, Bloebaum RD. 1999. Loading conditions and cortical bone construction of an artiodactyl calcaneus. J Exp Biol 202 (Pt 22):3239–3254.

Taylor AF, Saunders MM, Shingle DL, Cimbala JM, Zhou Z, Donahue HJ. 2007. Mechanically stimulated osteocytes regulate osteoblastic activity via gap junctions. Am J Physiol Cell Physiol 292:C545–C552.

Tommerup LJ, Raab DM, Crenshaw TD, Smith EL. 1993. Does weight-bearing exercise affect non-weight-bearing bone? J Bone Miner Res 8:1053–1058.

Turner AS, Mills EJ, Gabel AA. 1975. In vivo measurement of bone strain in the horse. Am J Vet Res 36:1573–1579.

Turner CH, Warden SJ, Bellido T, Plotkin LI, Kumar N, Jasiuk I, Danzig J, Robling AG. 2009. Mechanobiology of the skeleton. Sci Signal 2:pt3.

Vajda EG, Kneissel M, Muggenburg B, Miller SC. 1999. Increased intracortical bone remodeling during lactation in beagle dogs. Biol Reprod 61:1439–1444.

Van Bezooijen RL, Roelen BA, Visser A, van der Wee-Pals L, de Wilt E, Karperien M, Hamersma H, Papapoulos SE, ten Dijke P, Lowik C. 2004. Sclerostin is an osteocyte-expressed negative regulator of bone formation, but not a classical bmp antagonist. J Exp Med 199:805–814.

van Oers RF, Ruimerman R, Tanck E, Hilbers PA, Huiskes R. 2008. A unified theory for osteonal and hemi-osteonal remodeling. Bone 42:250–259.

Vashishth D, Verborgt O, Divine G, Schaffler MB, Fyhrie DP. 2000. Decline in osteocyte lacunar density in human cortical bone is associated with accumulation of microcracks with age. Bone 26:375–380.

Vatsa A, Breuls RG, Semeins CM, Salmon PL, Smit TH, Klein-Nulend J. 2008. Osteocyte morphology in fibula and calvaria—is there a role for mechanosensing? Bone 43:452–458.

Weinbaum S, Guo P, You L. 2001. A new view of mechanotransduction and strain amplification in cells with microvilli and cell processes. Biorheology 38:119–142.